Ab Initio Calculation of Proton−Hydrocarbon Scattering Cross Sections

Robert J. Buenker,* Yan Li, and Gerhard Hirsch

Fachbereich 9, Theoretische Chemie, Bergische Universität, Gesamthochschule Wuppertal, Gaussstrasse 20, D-42097 Wuppertal, Germany

Mineo Kimura†

School of Allied Health Sciences, Yamaguchi University, Ube, Yamaguchi 755, Japan

Received: February 11, 1998; In Final Form: June 8, 1998

The prediction of scattering cross sections for atom−molecule collisions by means of ab initio electronic structure methods is discussed with reference to recent calculations for the proton−methane and proton−ethyne systems. Potential energy surfaces and nonadiabatic coupling elements are computed employing the multireference single- and double-excitation configuration interaction (MRD-CI) method. These data are then taken as input for either a semiclassical or a fully quantum treatment to compute scattering cross sections for both elastic and inelastic processes. The role of molecular symmetry in determining both the shapes of the potential curves and the radial coupling elements between different channels is discussed and illustrated with numerous examples. Nonadiabatic couplings cause transitions between molecular states and their effect on the computed differential and total cross sections for charge transfer and elastic processes for different proton approaches are compared for the two collision systems.

I. Introduction

Although reliable calculations of scattering cross sections for atom−atom collisions are becoming commonplace in the literature at the present time,[1−4] surprisingly little work has appeared which describes the analogous quantities for collisions of atoms with molecules. One might think that the degree of complexity increases rapidly with the number of atoms in the molecular target, but this is not necessarily the case, particularly if attention is restricted to fairly high-energy interactions for which there is very little time for geometrical relaxation. Since relatively small molecules are abundant in some astrophysical environments,[5,6] as well as in fusion reactors and plasma-chemistry atmospheres,[7] it is quite important to compile cross section data for proton collisions with such systems in a wide range of energy. Both elastic and inelastic processes of this type need to be studied, whereby in the latter category charge transfer reactions are especially interesting for experimentalists.

To pursue this type of research theoretically, it is necessary to merge two fundamentally different types of computational methods. First, potential energy surfaces and corresponding coupling matrix elements must be predicted with suitably high accuracy. Because of the wide variation in the electronic structure of the combined target−projectile system, it is important to employ highly correlated electronic wave functions to achieve this goal at all satisfactorily, and for this purpose the multireference configuration interaction approach is especially well suited. The resulting computational data then need to be supplied as input for scattering cross section calculations, which can be carried out with either a semiclassical or a quantum approach, depending on the collision energy range of interest. The semiclassical MO expansion method assumes a straight-line trajectory of the incident ion such as a proton and is applicable for collision energies greater than about 50 eV. The relative motion of the nuclei is treated classically, while the electronic motion is described quantum mechanically. For lower-energy processes a fully quantum mechanical representation is preferred. The total wave function is then a product of electronic and nuclear factors, which upon substitution into the stationary Schrödinger equation leads to coupled, second-order differential equations for the nuclear motion. In both cases transitions between molecular states are driven by nonadiabatic couplings, which again are to be supplied by high-quality ab initio electronic structure calculations.

Recently several such applications have been reported for proton collisions with the key organic molecules, methane CH_4[8] and ethyne C_2H_2.[9] These calculations have been successful in elucidating the main features of the experimental cross-section data for these two systems, but they also illustrate in a more general manner how such a combination of ab initio CI and scattering dynamics calculations can be carried out in practice. It is especially important to know which simplifications can be made in the overall theoretical treatment to achieve a suitable level of accuracy with acceptable computational expenditures. In the following we will describe in some detail how both essential parts of these calculations have been carried out in the above two examples.[8,9] Then key features of the electronic structure of the CH_5^+ and $C_2H_3^+$ molecular ions will be discussed, including potential surfaces for a number of the lowest-lying states in both systems and the radial coupling matrix elements connecting them. Finally, the results of the scattering cross-section calculations will be presented and analyzed in terms of the computed electronic structure characteristics for each of the proton−molecule collision systems.

II. Configuration Interaction Treatment

From the standpoint of electronic structure calculations, the goal is to provide as accurate as possible a description of the

* e-mail: buenker@wrcs1.urz.uni-wuppertal.de; fax: +49-202-4392581.
† e-mail: mineo@rikax1.riken.go.jp; fax: +81-836-22-2130.

S1089-5639(98)01086-X CCC: $15.00
Published on Web 08/15/1998

low-lying states of the combined atom−target molecular system. It is necessary to go beyond the Born−Oppenheimer approximation in order to obtain a suitably quantitative picture of the collision processes of interest, but the starting point for such calculations nonetheless involves a complete separation of the electronic and nuclear motion. Adiabatic electronic wave functions for a variety of low-lying states need to be computed for suitably wide variations in the nuclear conformation. A highly flexible treatment of electron correlation effects is thus essential to achieve a balanced treatment for all interesting electronic states over the entire range of internuclear distance required to provide sufficiently accurate input data for the ensuing scattering calculations. A full configuration interaction (full CI) treatment is capable of meeting this challenge, but only if a suitably flexible atomic orbital (AO) basis is employed. For many-electron systems such a conceptually straightforward method is not feasible, but it can be approached in accuracy by employing a multireference description of the key electronic states. The CI space is restricted to configurations which differ by at most a double substitution with respect to any one of the reference species as long as an orthonormal one-electron basis is used to construct the individual Slater determinants. Such an approach (MRD-CI) has been used successfully to describe a wide variety of electronic structure problems since its introduction in the early 1970s.[10,11]

For the hydrocarbon ion calculations under discussion, the AO basis has been chosen as follows. The (9s5p1d) primitive set of Cartesian Gaussians given by Huzinaga[12] for the carbon atom has been employed in a [5s3p1d] contraction constructed by Dunning.[13] Since both methane and ethyne have low-lying Rydberg excited states, additional diffuse functions were added, however, two of s-type (with exponents of 0.023 and 0.0055) and two of p-type (0.021 and 0.0049). A d-type function with 0.015 exponent has also been employed in the C_2H_2/H^+ calculations. The hydrogen basis, also due to Huzinaga and Dunning, is (5s1p) contracted to [3s1p]. The resulting AO basis is thus of double-ζ-plus-polarization (DZP) quality.

The reference configurations are chosen on the basis of a series of preliminary MRD-CI calculations at representative nuclear geometries, with the goal of including all terms which occur with a moderately large coefficient somewhere along the potential surface of interest. In the present case attention has been restricted to states which dissociate to the lowest asymptotes of $CH_4 + H^+$ or $CH_4^+ + H$ and corresponding limits for the proton−ethyne system. The union of all such key configurations found at any geometry is then employed as a common reference set in the final stage of the calculations. Because primary interest lies in relatively high collision energies (ca. 1 keV), the nuclear arrangements of the CH_4 and C_2H_2 targets can be safely fixed at their respective ground-state equilibrium geometries. For methane three proton approaches have been considered: (a) along a CH bond from the hydrogen side (C_{3v} symmetry), (b) bisecting a CH_2 angle (C_{2v}), and (c) along a CH bond from the opposite direction as (a). The computed potential curves and couplings for the C_{2v} and face-centered proton approaches (b) and (c) are found to be quite similar, as is understandable from the fact that in both cases there is a relatively unobstructed path to the carbon atom. This similarity persists in the subsequent scattering cross section calculations, and thus in the following discussion no further mention of the face-centered C_{3v} approach will be made.

For ethyne only proton approaches along the linear axis ($C_{\infty v}$) and perpendicular to the midpoint of the molecule (C_{2v}) have been considered. The orthonormal (MO) one-electron basis is generated in all cases by carrying out a closed-shell Hartree−Fock calculation for the lowest closed-shell electronic configuration. Because the overall systems have a positive charge, the diffuse virtual MOs are good approximations to Rydberg orbitals of the neutral target.[14] The MRD-CI calculations are carried out with the Table-CI algorithm[15−17] which enables efficient handling of the complex open-shell relationships which arise in computing the CI Hamiltonian matrix. Finally, a standard method[10,11] is employed to identify weakly interacting configurations. These are not included in the final CI secular equations, but their effect on the corresponding energy eigenvalues is then estimated by perturbation theory. Similarly the influence of higher than double excitations on the calculated energies is estimated by means of the multireference analogue of the Langhoff−Davidson correction.[18−20]

The electronic wave functions obtained with the above procedure are then employed to calculate a variety of molecular properties. For the purpose of the ensuing scattering cross-section calculations, the most important of these are the nonadiabatic coupling matrix elements, which are computed by numerical differentation of the MRD-CI wave functions.[21,22] Electric-dipole transition moments are also calculated as well as the angular momentum matrix elements which are needed to describe rotational coupling of the Born−Oppenheimer wave functions. These results are obtained analytically.

III. Collision Dynamics and Scattering Cross Section Calculations

In the present calculations, we have adopted two types of theoretical approaches, namely, a semiclassical and a fully quantum mechanical treatment. For a heavy-particle collision at an energy above 100 eV, the de Broglie wavelength for the relative motion of the heavy particles is small compared with atomic dimensions, and the relative energy of the nuclei is larger than the energy loss due to the inelastic-scattering process. Under these circumstances, the nuclei can be assumed to move classically along some trajectory. The electrons experience an intrinsically time-dependent force field due to the moving nuclei, and, hence, the electronic wave function must satisfy a time-dependent Schrödinger equation. Although this semiclassical picture is an approximation to the fully quantum-mechanical counterpart, the merit of using such a representation is to provide an intrinsically simpler picture of the collision dynamics and to simplify the computations.[1]

Semiclassical Approach. A semiclassical molecular orbital (MO) expansion method with a straight-line trajectory of the incident ion has been employed to study the collision dynamics above 100 eV. In this approach, the relative motion of the heavy particles is treated classically, while electronic motions are treated quantum mechanically. The total scattering wave function is expanded in terms of products of a molecular electronic state and atomic-type electron translation factors (ETFs), in which the inclusion of the ETF satisfies the correct scattering boundary condition. By substituting the total wave function into the time-dependent Schrödinger equation and retaining the ETF correction up to first order in the relative velocity between the collision partners, one obtains a set of first-order coupled equations in time t. Transitions between the molecular states are driven by nonadiabatic couplings. In the present study, rotational coupling has been assumed to be of negligible importance because of the emphasis on high-energy collisions. Explicit tests carried out for the C_2H_2/H^+ system with semiclassical calculations employing rotational couplings for up to four channels have verified that such effects are of secondary importance for electron-capture processes.

By solving the coupled equations numerically, one obtains the scattering amplitudes for the transitions: the square of the amplitude gives the transition probability, and integration of the probability over the impact parameter gives the cross section. This approach has been employed to investigate electron capture in collisions of H^+ ions with the C_2H_2 molecule. Hence, the molecular states included in the dynamical calculations are the two sets of states separating to the initial $H^+ + C_2H_2$ channel, various electron capture $H + C_2H_2^+$, and target-excitation $H^+ + C_2H_2$* channels.

Quantum Approach. A fully quantum mechanical representation of the MO expansion method has also been employed, that is, one in which dynamical transitions are driven by nonadiabatic couplings. The total wave function for scattering is described as a product of the electronic, nuclear wave functions and ETFs. Substitution of the total scattering wave function into the stationary Schrödinger equation yields coupled, second-order differential equations for nuclear wave functions $\chi^a(R)$. It is computationally convenient to solve the coupled equations in a diabatic representation.[1,9] The transformation from the adiabatic to the diabatic representation can be readily achieved through a unitary transformation matrix, $\mathbf{C}(R)$. In this representation the nuclear wave function for the heavy particles is defined as $\chi^d(R) = \mathbf{C}^{-1}\chi^a(R)$, and the diabatic potential matrix is $\mathbf{V}^d = \mathbf{C}^{-1}\mathbf{V}^a\mathbf{C}$, where $\mathbf{V}^a$ is the adiabatic potential matrix. The resulting coupled equations for $\chi^d(R)$ are given in matrix form as

$$[(2\mu)^{-1}\nabla_R^2\mathbf{I} - \mathbf{V}^d(R) + E\mathbf{I}]\,\chi^d(R) = 0 \qquad (1)$$

where μ is the reduced mass of the system, $\mathbf{I}$ is the identity matrix, and $\mathbf{V}^d$ is the diabatic potential matrix. The coupled equations (1) are solved numerically to obtain the scattering $\mathbf{S}^l$ matrix for each partial wave l.[1] The differential cross section is then obtained from the standard formula

$$\frac{d\sigma(\theta)}{d\Omega} = \frac{1}{4k^2}\left[\sum_l (2l+1)\{\delta_{if} - S_{if}^l\}P_l(\cos\theta)\right]^2 \qquad (2)$$

where S_{if}^l is the scattering **S**-matrix element for partial wave l, θ is the scattering angle in center-of-mass coordinates, and k is the momentum of the projectile with collision energy $E = k^2/2$. Integration over all angles gives the total cross section. In the present calculations, we have employed two- and three-state close-coupling treatments with molecular orbitals (MOs) corresponding to the initial $H^+ + CH_4$ and $H^+ + C_2H_2$ and electron capture $H + CH_4^+$ and $H + C_2H_2^+$ channels.

IV. Results of the Electronic Structure Calculations

Potential energy curves for the CH_4/H^+ and C_2H_2/H^+ collisions are shown in Figures 1a,b and 2a,b, respectively, while Tables 1 and 2 contain a description of the states involved and the symmetry relations for the different approaches. At large proton−target separations, the two systems differ in the relative energetics of the lowest pair of charge transfer states. The adiabatic ionization potential of methane is 0.6 eV smaller than the H atom IP, but the value for vertical ionization exceeds it. Since the ethyne adiabatic IP is 1.58 eV lower than that for CH_4, nuclear relaxation effects are not sufficient to reverse the order of charge transfer states in this case, however. The basic premise of the present treatment is that, when the collision energy is high (keV range), the target system in the initial channel (neutral methane or ethyne in their respective ground-state equilibrium conformations) does not have time to relax significantly as the proton makes a close approach.

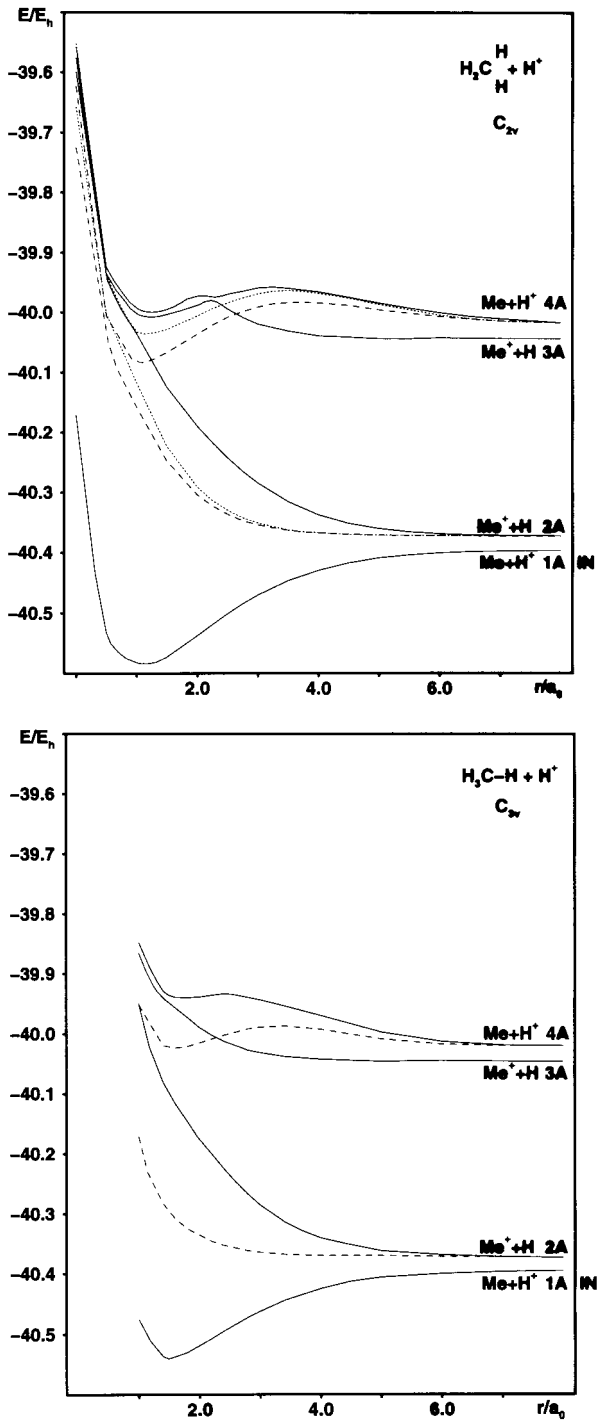

Figure 1. Potential energy curves for the $(CH_4 + H)^+$ system. (a,top) C_{2v} approach bisecting a CH_2 angle with solid lines for $^1A_1$, dashed lines for $^1B_2$ and dotted lines for $^1B_1$ states; r is the distance between the proton and the midpoint of the nearest H−H pair. (b, bottom) C_{3v} approach along a C−H bond with solid lines for $^1A_1$ and dashed lines for E states; r is the distance between the proton and the nearest H atom of CH_4. See Table 1 for a description of the states.

Under these conditions the initial channel for proton−methane scattering has an asymptotic energy which is 0.022 E_h lower than the lowest charge-transfer counterpart (Figures 1a,b). As the proton enters the charge cloud of the methane target, this energy difference increases dramatically, particularly in the C_{2v} approach where the H^+ is relatively free to penetrate, but also for C_{3v} geometry. The same is true for the C_2H_2/H^+ $C_{\infty v}$ initial

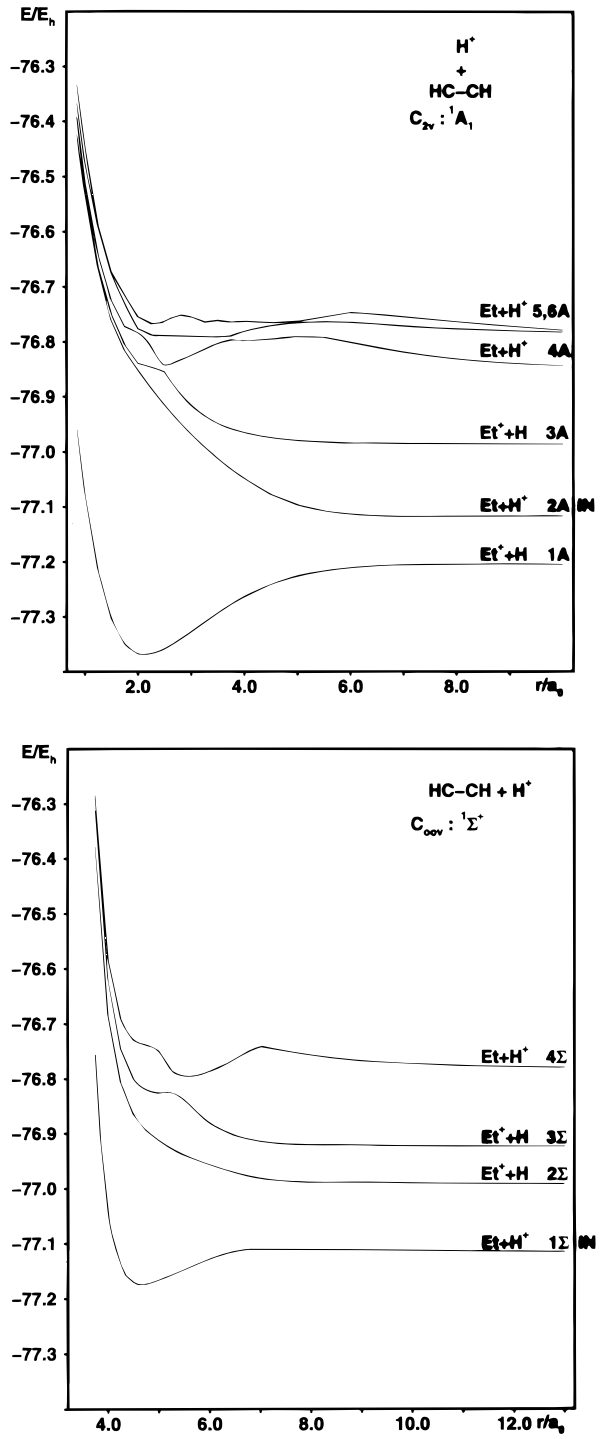

Figure 2. Potential energy curves for the $(C_2H_2 + H)^+$ system. (a, top) C_{2v} approach perpendicular to the C−C bond; only the resulting $^1A_1$ states are shown; r is the distance between the proton and the midpoint of the C−C bond. (b, bottom) $C_{\infty v}$ approach along the C_2H_2 axis with only $^1\Sigma^+$ states shown; r is the distance between the proton and the nearest H atom of C_2H_2. See Table 2 for a description of the states.

channel (Figure 2b), but the behavior for the analogous C_{2v} approach is quite different (Figure 2a). Such distinctions can be understood at least qualitatively from symmetry considerations. In the proton−methane collision system, the initial channel is characterized by a closed-shell singlet electronic configuration, and the lowest charge-transfer channel ($CH_4^+ +$ H) also has a component of the same ($^1A_1$) symmetry in both the C_{3v} and C_{2v} approaches. At short proton−methane separations the interaction between these two states of lowest energy causes the lower potential curve to drop sharply ($CH_4 + H^+$) while pushing the charge-transfer state higher in energy, both in the C_{2v} and the C_{3v} approaches (Figure 1a,b).

In the proton−ethyne collisions, symmetry plays a more differentiating role, as can be seen from the summary in Table 2. In the center column the molecular states for C_2H_2 and $C_2H_2^+$ ($D_{\infty h}$) are listed. By adding H or H^+, respectively, on a collinear axis, the symmetry reduces to $C_{\infty v}$ and the initial channel IN corresponds to a $^1\Sigma^+$ state. Other $^1\Sigma^+$ states arise from the molecular ions $C_2H_2^+$ ($3\sigma_g \rightarrow \infty$) or $C_2H_2^+$ ($2\sigma_u \rightarrow \infty$), for example, but not from the $1\pi_u \rightarrow \infty$ ionization. The situation is different for the perpendicular approach, which reduces the symmetry to C_{2v} so that the initial state becomes $^1A_1$. Further $^1A_1$ states arise from ionization out of the $1\pi_u$ or $3\sigma_g$ orbitals, but not for $2\sigma_u \rightarrow \infty$, for example. Analogous differences between the collinear and perpendicular approaches for target excitation to Rydberg orbitals can also be seen from Table 2. Hence, the initial (IN = 2A) and charge transfer (1A) channels are of the same symmetry ($^1A_1$) for the C_{2v} approach and thus the lower-energy channel, which corresponds to charge transfer in this case, has a strongly attractive potential curve, while that corresponding to the initial channel is repulsive, in stark contrast to the situation for the CH_4/H^+ collision system. For the linear approach of the proton to the ethyne target, the lowest-energy (charge transfer) channel has $^{3,1}\Pi$ symmetry, whereas the initial channel IN is of $^1\Sigma^+$ type. As a consequence, the initial channel is characterized by an attractive potential curve and cannot reach the lower charge-transfer channel $^{3,1}\Pi$ by a radial coupling mechanism.

In the CH_4/H^+ system the relatively strong interaction that takes place between the initial and charge-transfer channels can also be seen from another feature of the potential energy diagrams (Figure 1a,b). The CH_4^+ ion is triply degenerate ($^2T_2$), but in the field of the additional hydrogen atom its components split apart. The states of $^2B_1/^2B_2$ (C_{2v}) or E symmetry (C_{3v}) are not affected by the initial channel at small internuclear distances by virtue of the distinction in symmetry. As a consequence their potential curves (dashed and dotted lines in Figure 1a,b) are less repulsive than the CH_4^+ ($^2A_1$)−H counterpart for both the C_{3v} and C_{2v} approaches.

The above discussion emphasizes that the initial and charge-transfer channels do not undergo an avoided crossing in either of the proton−molecule systems under discussion. They do exhibit Demkov-type coupling, however, at least in the three cases where pairs of states of the same symmetry are involved; i.e., there is some mixing between the respective diabatic states as the H^+ projectile approaches the target molecule. As we shall see later when discussing the computed scattering cross sections, this fact is quite important in understanding the mechanisms for charge transfer in the two collision systems.

There is a large energy gap between the lowest two channels of the CH_4/H^+ system and the next group of excited states. Methane is a saturated hydrocarbon and its lowest excited states are Rydberg in nature (see Table 1). The present CI treatment places the $1t_2 \rightarrow 3s$ vertical excitation energy at 10.1 eV. The first excited $CH_4^+ +$ H channel lies 0.6 eV lower, again with the CH_4 nuclear geometry fixed at the equilibrium conformation of the neutral ground state. This corresponds to a $2a_1$ (2s) → $1t_2$ (2p) inner-valence transition of the molecular ion. The singlet potential curves associated with both these channels vary relatively slowly with the H−CH_4 internuclear distance in both the C_{3v} and C_{2v} approaches. The repulsive charge-transfer state discussed first intersects these excited channels at short r values

TABLE 1: Description of $(CH_4 + H)^+$ Systems in Both C_{2v} and C_{3v} Symmetry[a]

bisecting a CH_2 angle				along a C−H bond		
channel with $^1A_1$	component states	combination in C_{2v}	states of CH_4 (Me) and CH_4^+ (Me^+) in T_d	combination in C_{3v}	component states	channel with $^1A_1$
IN = 1A	$^1A_1$	$H^+ + Me$ ($^1A_1$)	Me(Ψ; $^1A_1$)	$H^+ + Me$ ($^1A_1$)	$^1A_1$	1A = IN
2A	$^{1,3}(A_1, B_1, B_2)$	$H + Me^+$ ($^2(A_1, B_1, B_2)$)	Me^+ ($1t_2 \rightarrow \infty$; $^2T_2$)	$H + Me^+$ ($^2(A_1, E)$)	$^{1,3}(A_1, E)$	2A
3A	$^{1,3}A_1$	$H + Me^+$ ($^2A_1$)	Me^+ ($2a_1 \rightarrow \infty$; $^2A_1$)	$H + Me^+$ ($^2A_1$)	$^{1,3}A_1$	3A
4A	$^{1,3}(A_1, B_1, B_2)$	$H^+ + Me(^{1,3}(A_1, B_1, B_2))$	$Me(1t_2 \rightarrow 3s_{ryd}$; $^{1,3}T_2)$	$H^+ + Me$ ($^{1,3}(A_1, E)$)	$^{1,3}(A_1, E)$	4A

[a] The configuration of the initial channel's CH_4 is $\Psi = 1a_1^2\, 2a_1^2\, 1t_2^6$. With respect to the initial channel IN = 1A, the channels 2A (asymptotically at 0.6 eV above IN) and 3A (9.5 eV) represent charge transfer, channel 4A (10.3 eV) target excitation.

TABLE 2: Description of $(C_2H_2 + H)^+$ Systems in Both C_{2v} and $C_{\infty v}$ Symmetry[a]

perpendicular approach				linear approach		
channel with $^1A_1$	component states	combination in C_{2v}	states of C_2H_2 (Et) and $C_2H_2^+$ (Et^+) in $D_{\infty h}$	combination in $C_{\infty v}$	component states	channel with $^1\Sigma^+$
1A	$^{1,3}(A_1, B_2)$	$H + Et^+$ ($^2(A_1, B_2)$)	Et^+ ($1\pi_u \rightarrow \infty$; $^2\Pi_u$)	$H + Et^+$ ($^2\Pi$)	$^{1,3}\Pi$	
IN = 2A	$^1A_1$	$H^+ + Et$ ($^1A_1$)	Et (Ψ; $^1\Sigma_g^+$)	$H^+ + Et$ ($^1\Sigma^+$)	$^1\Sigma^+$	1Σ = IN
3A	$^{1,3}A_1$	$H + Et^+$ ($^2A_1$)	Et^+ ($3\sigma_g \rightarrow \infty$; $^2\Sigma_g^+$)	$H + Et^+$ ($^2\Sigma^+$)	$^{1,3}\Sigma^+$	2Σ
	$^{1,3}B_1$	$H + Et^+$ ($^2B_1$)	Et^+ ($2\sigma_u \rightarrow \infty$; $^2\Sigma_u^+$)	$H + Et^+$ ($^2\Sigma^+$)	$^{1,3}\Sigma^+$	3Σ
4A	$^{1,3}(A_1, B_2)$	$H^+ + Et$ ($^{1,3}(A_1, B_2)$)	$Et(1\pi_u \rightarrow 3s_{ryd}$; $^{1,3}\Pi_u)$	$H^+ + Et(^{1,3}\Pi)$	$^{1,3}\Pi$	
5A, 6A	$2 \times {}^{1,3}(A_1, B_2)$	$H^+ + Et$ ($2 \times {}^{1,3}(A_1, B_2)$)	$Et(1\pi_u \rightarrow 3p\pi_{ryd}$; $^{1,3}(\Sigma_g^+, \Sigma_g^-, \Delta_g))$	$H^+ + Et(^{1,3}(\Sigma^+, \Sigma^-, \Delta))$	$^{1,3}(\Sigma^+, \Sigma^-, \Delta)$	4Σ
	$^{1,3}(A_2, B_1)$	$H^+ + Et$ ($^{1,3}(A_2, B_1)$)	$Et(1\pi_u \rightarrow \infty$; $3p\sigma_{ryd}$; $^{1,3}\Pi_g)$	$H^+ + Et(^{1,3}\Pi)$	$^{1,3}\Pi$	
7A	$^{1,3}A_1$	$H + Et^+$ ($^2A_1$)	Et^+ ($2\sigma_g \rightarrow \infty$; $^2\Sigma_g^+$)	$H + Et^+$ ($^2\Sigma^+$)	$^{1,3}\Sigma^+$	5Σ

[a] The configuration of the initial channel's C_2H_2 is $\Psi = 1\sigma_g^2\, 1\sigma_u^2\, 2\sigma_g^2\, 2\sigma_u^2\, 3\sigma_g^2\, 1\pi_u^4$. With respect to the initial channel IN = 2A = 1Σ, the channels 1A (asymptotically at 2.4 eV below IN), 3A = 2Σ (at 3.4 eV above IN), 3Σ (5.2 eV), and 7A = 5Σ represent charge transfer, the channels 4A (7.4 eV) and 5A, 6A = 4Σ (9.1 eV) target excitation.

at an energy of about 11 eV above the initial channel's asymptote (Figure 1a,b). As a result these excited channels have not been considered in detail in the associated scattering cross-section calculations for the proton−methane collision system.

The situation is more complex for the C_2H_2/H^+ system, however, because of the unsaturated nature of the ethyne target molecule. The second and third excited channels 2Σ and 3Σ are also of charge-transfer type, corresponding to ionization of C_2H_2 out of the relatively high-lying $3\sigma_g$ and $2\sigma_u$ MOs. At infinite separation the present calculations place the former's asymptotic energy only 3.4 eV above that of the initial channel (again with the C_2H_2 geometry fixed at its ground-state equilibrium conformation). It has a $^1\Sigma^+$ component for the linear approach of the proton (2Σ) and a $^1A_1$ counterpart (3A) for C_{2v} symmetry, allowing it to mix with the initial channel IN in both cases (see Table 2). The latter (IN) is more repulsive in the C_{2v} approach (Figure 2a,b) because of the interaction with the lowest charge-transfer channel 1A (which is forbidden by symmetry in $C_{\infty v}$), and this causes it to come much closer in energy to the $C_2H_2^+$ ($^2\Sigma_g^+$) + H channel at small r values in this arrangement than when the proton arrives along the linear C_2H_2 axis. On the other hand, the $^2\Sigma_g^+$ and $^2\Sigma_u^+$ $C_2H_2^+$ channels 2Σ and 3Σ can mix in linear symmetry but not for the corresponding C_{2v} proton approach, for which the perpendicular plane remains a symmetry element.

At still higher energy the next channel (4A) involves the $\pi \rightarrow$ 3s Rydberg excited state of ethyne. Its $^1\Pi_u$ symmetry allows it to mix with the charge-transfer channels below it for the C_{2v} proton approach but not in the collinear arrangement (Figure 2a,b). The $\pi \rightarrow 3p\pi$ C_2H_2 excitation produces the next $^1\Sigma^+/{}^1A_1$ channel (4Σ = 5,6A). Its vertical asymptotic energy is computed to be 9.1 eV above that of the initial channel. Its symmetry allows it to mix with the lower-lying 4A channel in the C_{2v} but not in the $C_{\infty v}$ proton approach. There is thus a fairly complicated series of avoided crossings in the $r = 2.0$−$2.5a_0$ range in C_{2v}. The $\pi \rightarrow 3p\pi$ excitations also produces a $^1\Delta_g$ and a $^1\Sigma_g^-$ state. In the same energy range there is also a $\pi \rightarrow p\sigma\, ^1\Pi_g$ state. The density of electronic states thus increases sharply beyond this energy range and the present calculations did not pursue the corresponding interactions. The $2\sigma_g \rightarrow \infty\ ^2\Sigma_g^+$ $C_2H_2^+$ + H charge-transfer channel has been computed, however, and is found to lie in the immediate neighborhood of the $\pi_u \rightarrow$ 3s,3p excitation channels.

Because of the large energy gap separating the lowest two CH_4/H^+ channels from the next most stable products, it was decided to concentrate on the elastic and charge-transfer processes involving these two channels. For this purpose radial nonadiabatic couplings have also been computed as a function of proton−target internuclear distance for both the C_{2v} and C_{3v} approaches (Figure 3). Since the initial channel has $^1A_1$ symmetry for both approaches, only the $^1A_1$ component of the $^1T_2$ charge-transfer state can mix with it via radial nonadiabatic coupling. As already discussed (Figure 1a,b) the initial and lowest charge-transfer channels do not undergo an avoided crossing with each other. Radial coupling can still occur, however, because of variations in the amount of mixing of their respective diabatic states as the proton−target distance is decreased (Demkov-type coupling).

The computed results show that the magnitude of this coupling element becomes large near $r = 6a_0$ in the C_{2v} approach (lower part of Figure 3) but remains quite small in the analogous range for the C_{3v} collision path (upper part of Figure 3). This distinction can be traced to the fact that the proton is freer to penetrate the methane charge cloud when it comes in along a bisector of a CH_2 angle than when it meets one of the methane H atoms head-on. As we shall see in the following section, this fact causes the total scattering cross section to be about 2 orders of magnitude larger for the C_{2v} proton−target approach (Figure 1a) than for the C_{3v} path in which the proton comes up against an H−C bond (Figure 1b). The radial coupling increases gradually as the proton−target separation decreases in the latter case, reaching a broad maximum near $r = 2.0a_0$ (Figure 3, top). By contrast, in the C_{2v} approach there is a sharp decline in the coupling (passing through a null value) after the large r maximum is reached (Figure 3, bottom), followed by an equally sharp increase to an

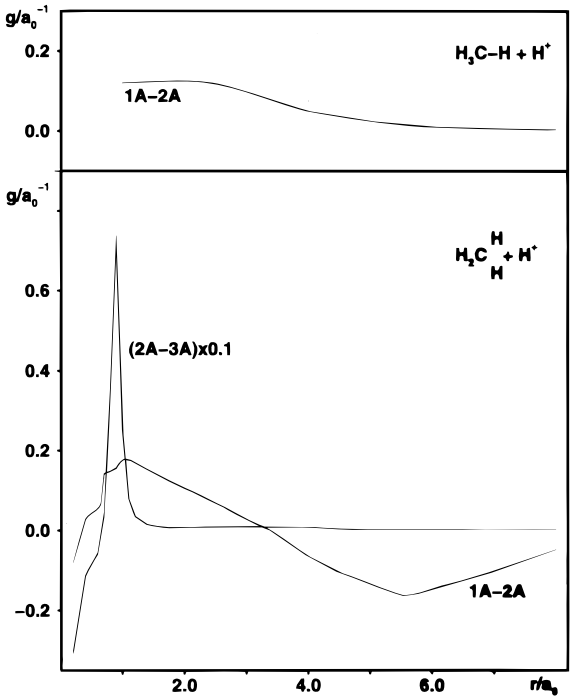

Figure 3. Radial coupling elements between different $^1A_1$ states of the $(CH_4 + H)^+$ system. Bottom: C_{2v} approach; r is the distance between the proton and the midpoint of the nearest H−H pair. Top: C_{3v} approach; r is the distance between the proton and the nearest H atom of CH_4.

inner maximum near $r = 1.0a_0$. The behavior of the radial coupling in the C_{3v} face-centered approach is similar to that found for the C_{2v} case, but the peak near $1.0a_0$ is much larger as a result of greater configuration mixing in this region.

To make the above argument easier to visualize, we have computed charge density contour plots for the initial channel in various key conformations (Figures 4a,b and 5a,b). In the C_{2v} approach the proton has a clear path to the carbon atom. The electronic charge moves outward to the proton as it travels from $r = 6.0$ (Figure 4a) to $r = 2.0a_0$ (Figure 4b). The corresponding changes in the initial and charge-transfer channels are already evident in the radial coupling matrix elements at $r = 8.0a_0$, and a maximum in this quantity is reached around $r = 5.5a_0$ (Figure 3, bottom). The analogous diagrams for the C_{3v} head-on approach show clearly that the charge distribution does not change as quickly in this case (Figure 5a,b). The electronic charge cloud surrounding the H atom of the nearest CH band is much less easily polarized as the proton approaches. The radial coupling element thus increases relatively slowly as r is decreased (Figure 3, top) and gradually reaches a plateau beginning around $r = 2.5a_0$.

As indicated above, the situation is notably more complicated in the $C_2H_3^+$ collision system because of the many low-lying channels available to it (Figure 6). In the $C_{\infty v}$ case the ground charge-transfer channel is of $^1\Pi$ symmetry and thus does not interact through radial coupling with the initial channel which is $^1\Sigma^+$. The most interesting effects are therefore found between the first two excited charge-transfer channels ($^2\Sigma_g^+$ and $^2\Sigma_u^+$ of $C_2H_2^+$) and the initial $C_2H_2 + H^+$ channel. The corresponding radial coupling elements are shown in Figure 6b ($1\Sigma-2\Sigma$ and $2\Sigma-3\Sigma$, respectively). Comparison with the potential energy curves (Figure 2b) makes clear why the $2\Sigma-3\Sigma$ radial couplings are notably larger than those for the $1\Sigma-2\Sigma$ pair of states. Similarly as for the CH_5^+ collision system, the dominant coupling scheme is of Demkov-type. The corresponding three

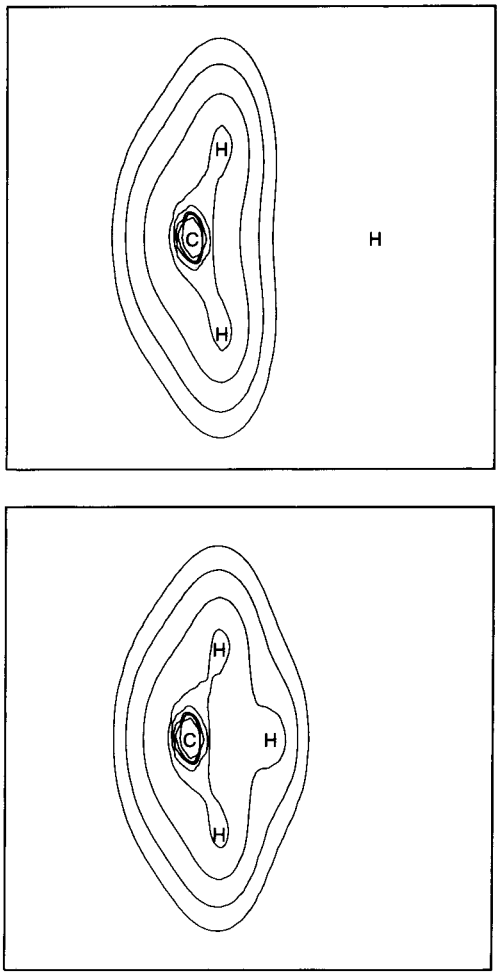

Figure 4. Charge density contours for the $(CH_4 + H)^+$ system in the H_2C-H plane of the C_{2v} approach with $r = 6a_0$ (a, top) and $r = 2a_0$ (b, bottom).

electronic states maintain their identities over a wide range of r, but the closer proximity of the 2Σ and 3Σ channels causes larger coupling than in the $1\Sigma-2\Sigma$ case.

For the perpendicular approach (C_{2v}) the initial channel (2A) has $^1A_1$ symmetry and is thus able to mix with both the ground (1A) and first excited (3A) charge-transfer channels. The corresponding radial couplings (Figure 6a) are again of Demkov-type, as is expected from the potential curves computed for these states (Figure 2a). The 2A−3A values are much larger, however, especially when the proton comes within $2.0a_0$ of the C_2H_2 midpoint. The situation is different for $r = 2.5a_0$, however. The 1A−2A coupling dominates in this range out to $r = 7a_0$ and is expected to be quite important for electron capture at high energies when the 2A−3A coupling dies off. In the next section we will see how these quantitative variations in the radial coupling matrix elements with decreasing proton−target separation determine the nature of the collision dynamics exhibited by the C_2H_2/H^+ system.

V. Computed Scattering Dynamics Results

A. Differential Cross Sections. *$H^+ + CH_4$.* The results of the differential cross section calculations have been shown earlier for C_{2v} symmetry (Figure 3a of ref 8) and for C_{3v} symmetry (Figure 4a of ref 8), for scattering angles 0−180° at 1.5 keV. Both electron capture and direct elastic scattering are considered. Several important features are summarized here and are discussed separately for small and large scattering angle regions: (i) $0° < \theta < 20°$ and (ii) $\theta > 20°$.

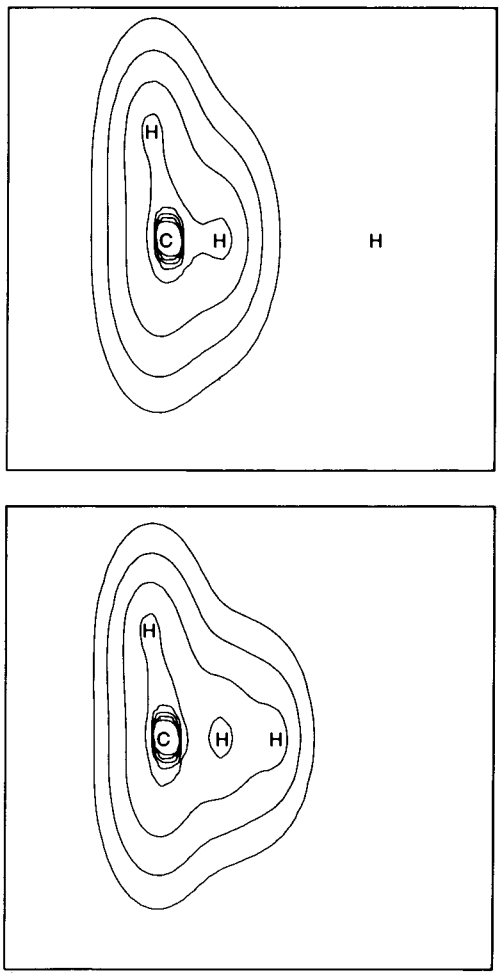

Figure 5. Charge density contours for the $(CH_4 + H)^+$ system in the HCH−H plane of the C_{3v} approach with $r = 6a_0$ (a, top) and $r = 2a_0$ (b, bottom).

For $0° < \theta < 20°$, the magnitude of the differential cross sections for electron capture for C_{2v} symmetry is larger than that for C_{3v} symmetry in this scattering angle domain. Events resulting in scattering angles of 10° or smaller correspond roughly to those of impact parameter larger than $2.0a_o$, in which case the projectile interacts only weakly with the constituent atoms in C_{2v} symmetry. By contrast, it experiences an isotropic field on its way between the three H atoms in C_{3v} symmetry. In addition, the small, high-frequency oscillations apparent for C_{3v} symmetry in both elastic and electron-capture differential cross sections may be attributable to quantum interferences. For C_{2v} symmetry, oscillatory structures are present, but they are much weaker and are irregular. For $\theta > 20°$, the elastic differential cross sections are smooth and flat with a near-constant value of 10^{-2} cm^2/sr as a function of scattering angle for C_{3v} head-on collisions (i.e., isotropic scattering). The corresponding electron capture values are at least an order of magnitude smaller and are also smooth except for a pronounced dip in the 45−75° range. The differential cross sections for the C_{2v} approach are much smaller, with mean values of 10^{-14} cm^2/sr, and they show numerous irregular oscillations, which are due to quantum interferences arising from strong two-state coupling. For C_{3v} symmetry, the isotropy is due to near head-on collisions between the projectile and the H atom in CH_4. The sharp dip in electron capture at 45° for 1.5 keV and 75° for 0.5 keV is considered to be due to rainbow scattering.

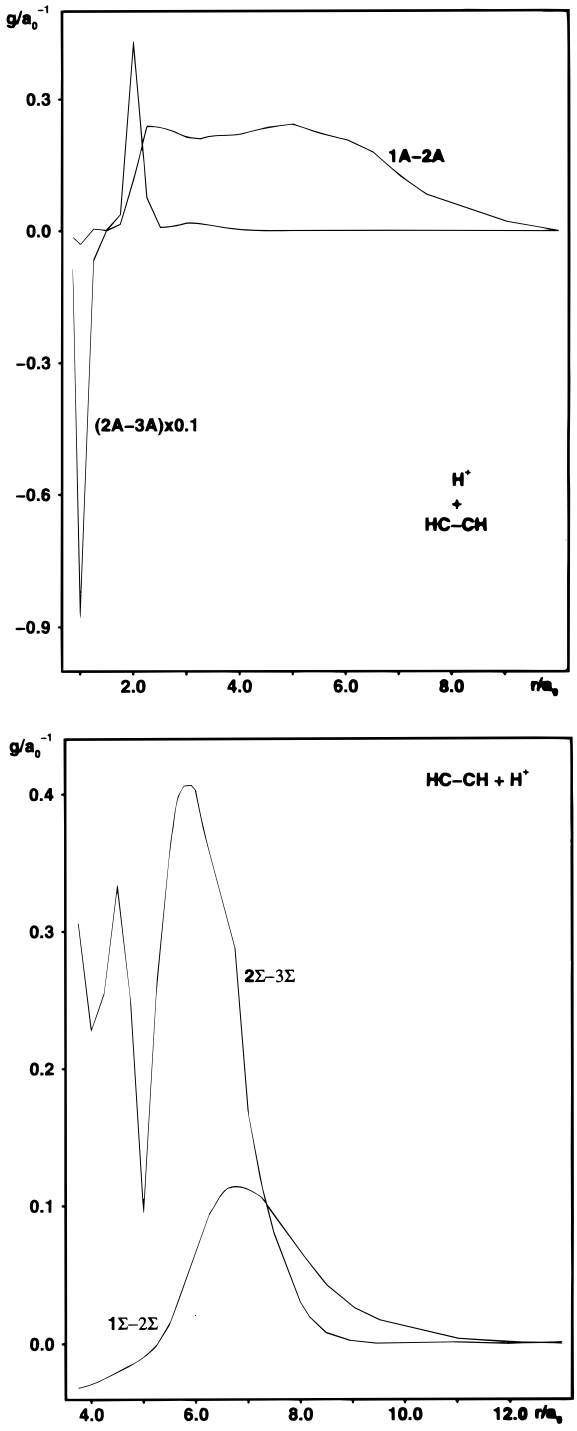

Figure 6. Radial coupling elements between different states of the $(C_2H_2 + H)^+$ system. (a, top) Coupling between two pairs of $^1A_1$ states in the C_{2v} approach; r is the distance between the proton and the midpoint of the C−C bond. (b, bottom) Coupling between two pairs of $^1\Sigma^+$ states in the $C_{\infty v}$ approach; r is the distance between the proton and the nearest H atom of C_2H_2.

At scattering angles near 180°, both elastic-scattering and electron-capture differential cross sections for C_{3v} symmetry drop sharply, suggesting the infrequent occurrence of actual head-on collisions. For C_{2v} symmetry, no significant characteristic is observed near this angle. In experiments, the measurement is carried out for the averaged differential cross section over all molecular geometries, not for a fixed well-identified geometry of a specific molecular configuration. Therefore, to properly compare our results with the measurements, we should employ an averaging procedure, the details

of which have been described earlier.[8,9] The averaged results are expected to be in notably better agreement with measurements at all scattering angles.

$H^+ + C_2H_2$. Differential cross sections for this system have been computed both for C_{2v} and $C_{\infty v}$ symmetries for scattering angles of 0−180° at 1.5 keV (Figures 3a and 3b of ref 9). Both electron capture and direct elastic scattering are included. For $0° < \theta < 10°$, the magnitude of the differential cross sections for electron capture in C_{2v} symmetry is slightly larger than that for $C_{\infty v}$ symmetry in this scattering angle domain. Events resulting in scattering angles of 10° or smaller correspond roughly to those of impact parameter larger than $2.0a_0$, which is too large to allow the projectile to interact strongly with any of the constituent atoms in $C_{\infty v}$ symmetry. The incoming H^+ ion just passes over the C_2H_2 molecule without strong interaction in this case, whereas it may feel a somewhat stronger effect from the C and H atoms for C_{2v} symmetry. For electron-capture differential cross sections for both C_{2v} and $C_{\infty v}$ symmetries, weak and irregular oscillatory structures are seen at small scattering angle below 10°.

The elastic differential cross section for $\theta > 10°$ is smooth and flat, with a nearly constant value of 1 cm^2/sr for a wide range of scattering angle (i.e., isotropic scattering) for $C_{\infty v}$ symmetry. In C_{2v} symmetry it has numerous irregular oscillations, but the mean value is also nearly constant, (0.1 cm^2/sr). The oscillations in C_{2v} symmetry are due to quantum interferences arising from strong two-state coupling, whereas for $C_{\infty v}$ symmetry, the isotropy is caused by nearly head-on collisions between the projectile and an H atom in C_2H_2. One remarkable feature in the linear approach, i.e., a sharp dip in electron capture at 6° for 1.5 keV which increases to two dips at 20° and 95° as the energy decreases, is due to rainbow scattering. For $\theta > 20°$, elastic scattering is always larger by at least an order of magnitude for $C_{\infty v}$ symmetry, while for C_{2v} symmetry, elastic scattering is generally larger than electron capture for all scattering angles except in the 25−45° region. Finally, at scattering angles near 180°, elastic-scattering differential cross sections rise rather sharply for C_{2v} symmetry, suggesting the occurrence of close collisions of the incoming H^+ ion with two carbon atoms at the center of the molecule. To a much weaker degree, a similar rise in the elastic-scattering differential cross section for linear symmetry can be seen, resulting from near collisions with a terminal hydrogen atom. Regular continuous oscillatory patterns are found in the elastic cross section for C_{2v} symmetry, while the elastic cross section is seen to be very flat and nearly constant in the linear approach.

Finally, in comparing the two systems it is clear that the two sets of differential cross sections for the head-on approach for H^+/CH_4 (C_{3v}) and H^+/C_2H_2 ($C_{\infty v}$) should show a high degree of similarity. Indeed, the respective elastic differential cross sections show similar flatness above 10°, and this situation does not change significantly even at lower collision energies. For electron-capture processes both sets of results exhibit a sharp dip due to rainbow scattering, although the angle at which this occurs is different. Otherwise, the electron-capture differential cross sections for both systems are found to be rather smooth. The corresponding C_{2v} proton approaches in both systems are marked by differential cross sections with rapid oscillations over the entire range of angle. These oscillations are also present at relatively low collision energies, and they are due to strong interactions with the other constituent atoms in the molecular targets. Similar oscillatory structures are also present in the electron capture differential cross sections, although they are not as prominent as those for the elastic processes. In summary, the differential cross sections show very similar trends for both systems when they are in comparable symmetric arrangements, reflecting the strength of the interactions involved.

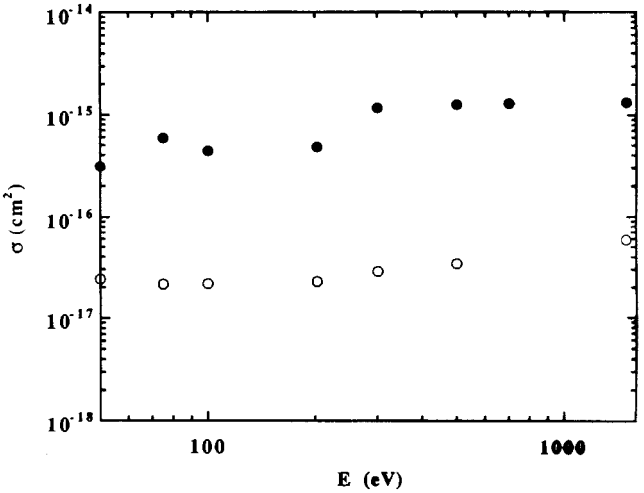

Figure 7. Total electron-capture cross sections σ for the $(CH_4 + H)^+$ system for C_{2v} (full circles) and C_{3v} (open circles) symmetries.

B. Total Cross Sections. $H^+ + CH_4$. Total integrated cross sections are illustrated separately for C_{2v} and C_{3v} symmetries in Figure 7. That of C_{2v} is larger than for C_{3v} in the entire energy range studied, reaching a maximum value of 1×10^{-15} cm^2 at 300 eV. Its C_{3v} counterpart is smoother and gradually increases to 6×10^{-17} cm^2 at 2000 eV. Rudd et al.[23] measured the electron capture cross sections above 5 keV and the present result at 2 keV appears to fit in reasonably well with their observations.

$H^+ + C_2H_2$. Total cross sections obtained by using the semiclassical calculation are illustrated separately for C_{2v} and $C_{\infty v}$ symmetries in Figure 8a,b. As stated, contributions from all channels, electron capture, electron capture with simultaneous target excitation, and target excitation, are included separately along with the summed total cross section in both symmetries. Total electron capture for the C_{2v} approach appears to possess a minimum at the lowest energy studied (near 30−40 eV) and gradually increases with energy, reaching a maximum value of 4.5×10^{-16} cm^2 around 4 keV, while that for $C_{\infty v}$ also increases just above the threshold and reaches a maximum, with a value of 2×10^{-16} cm^2 around 3 keV. The total electron-capture cross sections above 100 eV are larger by about a factor of 3 to 4 for C_{2v} symmetry than those for the linear approach. This is because near-zero angle scattering is responsible for most of the total cross section. For C_{2v} symmetry the total cross section is rather smooth as a function of energy, while that for $C_{\infty v}$ symmetry exhibits strong oscillatory structures in the entire energy region. These features are a manifestation of the coupling matrix elements and coupling schemes (Landau−Zener versus Demkov) discussed above.

VI. Conclusion

The accurate prediction of atom-molecule scattering cross sections requires a combination of two different computational techniques which are grounded in the Born−Oppenheimer approximation. A highly correlated treatment of the electronic structure of the target−projectile system must first be carried out on a point-by-point basis. This involves both the generation of multidimensional potential surfaces as well as various nonadiabatic coupling elements connecting them, in the present study primarily of the radial type. For relatively high-energy

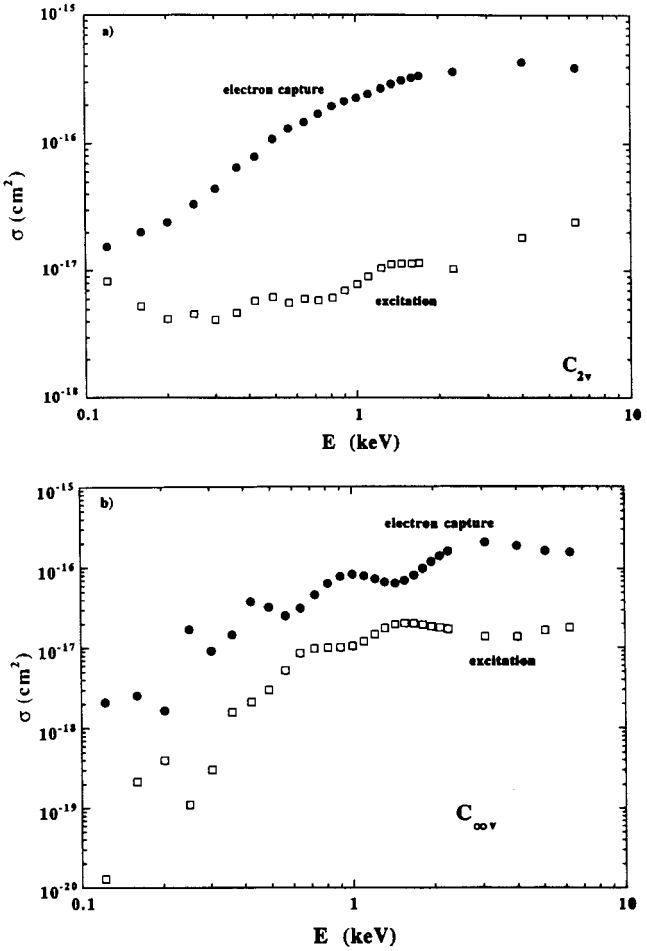

Figure 8. Total electron-capture cross sections σ for the $(C_2H_2 + H)^+$ system for C_{2v} (a) and $C_{\infty v}$ (b) symmetries.

scattering it is possible to simplify this part of the treatment by freezing the nuclear arrangement of the target molecule at its equilibrium geometry.

As the proton approaches from various directions, it is possible in many cases to anticipate changes in the total energy of the collision system on the basis of symmetry considerations. For example, the initial channel and one of the components of the lowest-lying charge-transfer channel in the proton−CH_4 system are of the same symmetry in both the C_{3v} and C_{2v} approaches. In both cases a deep minimum is observed for the (low-energy) initial channel, and a correspondingly repulsive curve for the other state. The effect is stronger in the C_{2v} approach because of the greater possibilities for the proton to penetrate the methane charge cloud in this nuclear arrangement. No avoided crossing occurs in either approach, but there is still a significant amount of radial coupling of Demkov-type whereby the mixing coefficients of the initial and charge-transfer states vary gradually. In the proton−C_2H_2 system the contrast between the linear and perpendicular approaches is much stronger because the initial and charge-transfer channels are of different symmetry in the former case, but of the same symmetry in the C_{2v} point group. The unsaturated character of the ethyne target produces a number of interesting effects for low-lying excited channels which are absent in the proton−methane collisions. In the perpendicular approach the initial channel undergoes a strong interaction with the $3\sigma_g^{-1}$ state of $C_2H_2^+$ and, at still shorter r values, with 3s Rydberg states of the neutral target.

To use the potential energy and radial coupling results of an ab initio CI treatment to obtain information about the cross sections for various elastic and inelastic processes, it is necessary to carry out scattering calculations at either the semiclassical or fully quantum level. In the former case, which is applicable for collision energies exceeding about 50 eV, the nuclear motion is treated classically, whereas the electronic structure is described with the aid of the ab initio data. For lower energies a fully quantum-mechanical representation is necessary, with the nuclear motion treated by means of coupled differential equations. The resulting scattering amplitudes are then squared to obtain transition probabilities, which upon integration over the impact parameter in the semiclassical treatment, or over angle in the quantum approach, yields the total scattering cross sections for the individual processes.

For low-angle scattering ($\theta \leq 20°$) of a proton off the CH_4 target, the differential cross section for electron capture is larger for the C_{2v} approach than for C_{3v}. The total cross sections for electron capture above 100 eV are 2 orders of magnitude larger in C_{2v} symmetry because of the dominance of low-angle scattering on this quantity. For $\theta > 20°$ both elastic and charge-transfer differential cross sections are smooth and flat (10^{-3} cm^2/sr) for C_{3v} symmetry, while there are numerous irregular oscillations with small mean values (10^{-14} cm^2/sr) for the C_{2v} approach. The isotropy in C_{3v} can be traced to the nearly head-on collisions of the proton with an H atom. The C_{3v} electron-capture differential cross sections have sharp dips in a narrow range of angle, however, which are considered to result from rainbow scattering.

For the proton−C_2H_2 system low-angle scattering, the electron-capture differential cross section for the perpendicular (C_{2v}) approach is only slightly larger than for $C_{\infty v}$ collisions. Above 100 eV the total electron-capture cross sections are thre to four times larger in C_{2v} symmetry because of the dominance of large impact−parameter scattering on this quantity. For larger angles ($\theta > 10°$) the elastic differential cross section has a nearly constant value of 1 cm^2/sr for the $C_{\infty v}$ approach. By contrast numerous irregular oscillations are computed in C_{2v} symmetry, with a mean value which is an order of magnitude smaller. Dips in the $C_{\infty v}$ electron-capture cross sections caused by rainbow scattering are also found. For $\theta > 20°$ elastic scattering dominates at all angles for the $C_{\infty v}$ approach, but in C_{2v} symmetry, charge-transfer cross sections exceed the elastic values in the 25−45° range. Total electron-capture cross sections rise gradually with the collision energy for the C_{2v} approach, whereas strong oscillations are noted when the proton arrives along the linear molecular axis. These distinctions can be understood in terms of the different coupling schemes involved (Landau−Zener versus Demkov). Finally, electron capture with target excitation is found to be less important than without for collision energies above 0.2 keV, but the opposite is true below this range for the C_{2v} approach.

Acknowledgment. The work was supported in part by the Deutsche Forschungsgemeinschaft (Grant Bu 450/7; R.J.B.) and by the U.S. Department of Energy, Office of Basic Energy Sciences through Rice University (M.K.). The financial support of the Fonds der Chemischen Industrie is also hereby gratefully acknowledged.

References and Notes

(1) Kimura, M.; Lane, N. F. In *Advances in Atomic and Molecular Physics*; Bates, D. R., Bederson, B., Eds.; Academic Press: New York, 1989; Vol. 26 p 79.

(2) Fritsch, W.; Lin, C. D. *Phys. Rep.* **1991**, *202*, 1.

(3) Kuntz, P. J. *Chem. Phys.* **1995**, *199*, 53.

(4) Errea, L. F.; Gorfinkiel, J. D.; Kryachko, E. S.; Macias, A.; Mendez, L.; Riera, A. *J. Chem. Phys.* **1997**, *106*, 172. Errea, L. F.; Gorfinkiel, J. D.; Macias, A.; Mendez, L.; Riera, A. *J. Phys. B* **1997**, *30*, 3855.

(5) Black, J. H.; Dalgarno, A. *Astrophys. J.* **1976**, *206*, 132.

(6) Geisler, G. E. *J. Geophys. Res.* **1967**, *72*, 81.

(7) Phaneuf, R. A.; Meyer, F. W.; McKnight, R. H. *Phys. Rev. A* **1974**, *17*, 534.

(8) Kimura, M.; Li, Y.; Hirsch, G.; Buenker, R. J. *Phys. Rev. A* **1995**, *52*, 1196.

(9) Kimura, M.; Li, Y.; Hirsch, G.; Buenker, R. J. *Phys. Rev. A* **1996**, *54*, 5019.

(10) Buenker, R. J.; Peyerimhoff, S. D. *Theor. Chim. Acta* **1974**, *35*, 33.

(11) Buenker, R. J.; Peyerimhoff, S. D. *Theor. Chim. Acta* **1975**, *39*, 217.

(12) Huzinaga, S. *J. Chem. Phys.* **1965**, *42*, 1293.

(13) Dunning, T. H., Jr. *J. Chem. Phys.* **1970**, *53*, 2823.

(14) Schwarz, W. H. E.; Buenker, R. J. *Chem. Phys.* **1976**, *13*, 153.

(15) Buenker, R. J. In *Proceedings of Workshop on Quantum Chemistry and Molecular Physics in Wollongong, Australia*; Burton, P., Ed.; University Press: Wollongong, 1980.

(16) Buenker, R. J. In *Studies in Physical and Theoretical Chemistry*, Vol. 21; *Current Aspects of Quantum Chemistry*; Carbó, R., Ed.; Elsevier: Amsterdam, 1981; p 17.

(17) Buenker, R. J.; Phillips, R. A. *J. Mol. Struct.* (*Theochem.*) **1985**, *123*, 291.

(18) Davidson, E. R. In *The World of Quantum Chemistry* Daudel, R.; Pullman, B., Eds.; Reidel: Dordrecht, 1974; p 17.

(19) Hirsch, G.; Bruna, P. J.; Peyerimhoff, S. D.; Buenker, R. J. *Chem. Phys. Lett.* **1977**, *52*, 442.

(20) Knowles, D. B.; Alvarez-Collado, J. R.; Hirsch, G.; Buenker, R. J. *J. Chem. Phys.* **1990**, *92*, 585.

(21) Hirsch, G.; Bruna, P. J.; Buenker, R. J.; Peyerimhoff, S. D. *Chem. Phys.* **1980**, *45*, 335.

(22) Buenker, R. J.; Hirsch, G.; Peyerimhoff, S. D.; Bruna, P. J.; Römelt, J.; Bettendorff, M.; Petrongolo, C. In *Studies in Physical and Theoretical Chemistry*, Vol. 21: *Current Aspects of Quantum Chemistry*; Carbó, R., Ed.; Elsevier: Amsterdam, 1981; p 81.

(23) Rudd, M. E.; DuBois, R. D.; Toburen, L. H.; Ratcliffe, C. A.; Goffe, T. V. *J. Chem. Phys.* **1983**, *28*, 3244.